LCC-0114
CBP Tech Note-280
February 2003

Linear Collider Collaboration Tech Notes

A Reduced Emittance Lattice for the NLC Positron Predamping Ring

Ina Reichel and Andrzej Wolski

Lawrence Berkeley National Laboratory
University of California
Berkeley, CA

Abstract: This is an updated version of [1]. In the design presented there the horizontal emittance of the extracted beam is too large by about 20%. In order to get the emittance down to the required value the quadrupole magnets in the dispersive regions in the ring are moved to provide J_x=1.1 which gives a small enough emittance. In addition a better model of the wiggler fields is used. The new design meets requirements. The lattice and dynamic aperture studies (assuming no machine errors) are presented.
.

CBP Tech-Note 280

LCC-0114

A Reduced Emittance Lattice for the NLC Positron Pre-Damping Ring

Ina Reichel, Andrzej Wolski
Lawrence Berkeley National Laboratory

February 24, 2003

Abstract

This is an updated version of [1]. In the design presented there the horizontal emittance of the extracted beam is too large by about 20%. In order to get the emittance down to the required value the quadrupole magnets in the dispersive regions in the ring are moved to provide $J_x = 1.1$ which gives a small enough emittance. In addition a better model of the wiggler fields is used. The new design meets requirements. The lattice and dynamic aperture studies (assuming no machine errors) are presented.

1 Introduction

The injector complex for the NLC uses identical main damping rings for each beam, that are specified to reduce the normalized emittance from 150 mm mrad horizontally and vertically, to below 3 mm mrad horizontally and 0.02 mm mrad vertically. With a repetition rate of 120 Hz, this damping can be achieved using a single ring for each beam. Design work leading to a suitable lattice for the main damping rings is described in [2]. The positron source is specified to produce a beam with edge emittance 30,000 mm mrad. It is not practicable to damp such a large emittance to the values required for injection into the main linac in a single ring. Furthermore, the main damping rings will not have the transverse acceptance required for a beam with such a large emittance.

The positron source parameters and the main damping ring specifications lead to the need for a pre-damping ring, that will reduce the emittance from 30,000 mm mrad, to below 100 mm mrad for injection into the main

Table 1: "External" parameters.

Bunches per train	N_b	192
Bunch-to-bunch spacing	$\tau_\mathrm{b}/\mathrm{ns}$	1.4
Kicker rise / fall time	$\tau_\mathrm{k}/\mathrm{ns}$	100
Collider repetition rate	f/Hz	120
Injected horizontal / vertical emittance (edge)	$\gamma\varepsilon_\mathrm{inj}/\mathrm{mm\,mrad}$	30,000
Injected emittance including transverse jitter	$\gamma\varepsilon_\mathrm{inj}/\mathrm{mm\,mrad}$	45,000
Extracted horizontal emittance (rms)	$\gamma\varepsilon_{x,\mathrm{ext}}/\mathrm{mm\,mrad}$	< 100
Extracted vertical emittance (rms)	$\gamma\varepsilon_{y,\mathrm{ext}}/\mathrm{mm\,mrad}$	< 100

damping ring. One significant difference between the pre-damping ring and the main damping rings is that the extracted emittance specification on the pre-damping ring is much more relaxed. Rapid damping is still required, but an equilibrium emittance of around 90 mm mrad or less will be sufficient. Also, it is not necessary to produce a flat beam, so the alignment tolerances and coupling correction will be much looser than in the main rings. However, the pre-damping ring will require a relatively large acceptance, which will impact the design of the lattice and its magnetic elements. Table 1 lists the external parameters.

The design presented in this note uses a 10-fold symmetric double-bend achromat (DBA) structure. The structure allows separation of the different components, so that the damping wiggler, injection / extraction systems, RF cavities and chicane are all placed in separate straights; this greatly assists lattice design, since the different cells can be optimized independently, and should also ease engineering constraints, for example in locating photon stops to absorb the synchrotron radiation from the dipoles and wiggler.

The design presented in [1] reduces the emittances to 127 mm-mrad (horizontal) and 70 mm-mrad (vertical). As can be seen the horizontal emittance is too large by about 20 %. One possibility to decrease this number is to increase the horizontal damping partition number J_x. An increase to about 1.1 was deemed sufficient.

The easiest way to change J_x is to change the rf frequency of the ring. Due to the ring being in a chain of accelerators this is not feasible. As a change in rf frequency mainly changes the orbit in the quadrupole magnets in dispersive regions one can obtain a similar results by moving those magnets and keeping the RF frequency fixed. To obtain a damping partition number of 1.1 in this ring requires the circumference to change by about 4.2 mm which corresponds to changing the position of the quadrupole magnets in the arcs by 1.5 mm.

The lattice was rematched after moving the magnets. At the same time the wiggler was changed to give a better representation of the real fields which in turn changed the focusing. To make tune adjustments easier a pair of quadrupole magnets was added to the wiggler cells.

After the basic lattice was matched the chromaticity was adjusted and harmonic sextupoles were used to decrease the detuning with amplitude.

2 Lattice Parameters

The lattice consists of ten double bend achromats (DBA). The main parameters of the lattice are given in Tab. 2; Tab. 3 lists the synchrotron radiation integrals and average beta functions. The basic double-bend achromat structure of a single cell is shown in Fig. 1. The dispersion is close to zero outside of the achromat. The wiggler generates only small amounts of residual dispersion. The achromat uses two quadrupole doublets, and three chromatic sextupoles. The harmonic sextupoles are located outside of the achromat. Use is made of the significant vertical focusing from the wiggler. In the previous design there was only a single quadrupole between the bend and the wiggler as the wiggler provided some focusing. However this made tuning the lattice difficult so another quadrupole was introduced. The beta functions are moderate, below 18 m horizontally and vertically throughout the cell. All quadrupoles in the achromat are horizontally offset by 1.5 mm.

Other types of cell are constructed for the RF cavities (Figure 2), chicane (Figure 3), injection (Figure 4) and extraction systems (Figure 5). Note that the structure and lattice functions in these different types of cell are very similar. The beta functions are slightly larger than in the wiggler cell, but still below 23 m. The geometry of the lattice is simplified by having the cells the same length, and the spacing of the dipoles the same in each case; thus, the layout is a regular decagon.

2.1 RF cell

There is more than sufficient space for four RF cavities. The RF system requires that the distance between the centerlines of the cavities is a whole number plus three-quarters of an RF wavelength. Adjacent cavities are separated by $3\,{}^{3}/_{4}$ wavelengths allowing pairs of cavities to be fed from a single klystron via a “magic T”. It is assumed at present that the cavities will be the same design as used in the main damping rings [3, 4], being HOM-damped structures based on the PEP-II design. Studies of instabili-

Table 2: Lattice parameters.

Energy	E/GeV	1.98
Circumference	C/m	230.93
Basic cell type		DBA
Basic cell length	$/\,\mathrm{m}$	23.09
Number of cells		10
Tunes (hor., vert., synch.)	Q_x, Q_y, Q_s	12.15, 6.19, 0.0098
Natural chromaticities (hor., vert.)	ξ_x, ξ_y	$-26.3, -15.6$
Normalized natural emittance	$\gamma\varepsilon_0/\mathrm{mm\,mrad}$	46
Damping times	$\tau_x, \tau_t, \tau_E/\mathrm{ms}$	3.5, 3.8, 2.0
Energy loss per turn in bends	$U_\mathrm{B}/\mathrm{keV}$	284
Energy loss per turn in wigglers	$U_\mathrm{W}/\mathrm{keV}$	519
Energy loss per turn total	U_0/keV	803
Assumed coupling	κ	10 %
Assumed inj. edge emittance	$\gamma\varepsilon_{inj}/\mathrm{mm\,mrad}$	30, 000
Assumed inj. edge em. incl. jitter	$\gamma\varepsilon_{inj}/\mathrm{mm\,mrad}$	45, 000
Extracted emittance (hor., vert.) (rms)	$\gamma\varepsilon_{ext}/\mathrm{mm\,mrad}$	49, 7.9
Momentum compaction	α	$1.69 \cdot 10^{-3}$
RF voltage	$V_\mathrm{rf}/\mathrm{MV}$	1.72
RF acceptance	ε_rf	1.5 %
RF frequency	$f_\mathrm{rf}/\mathrm{MHz}$	714
Harmonic number	h	550
Equilibrium energy spread (rms)	σ_δ	0.00089
Equilibrium bunch length (rms)	σ_z/mm	5.12

Table 3: Synchrotron radiation integrals and average beta-functions.

$I1$	0.39
$I2$	3.71
$I3$	0.98
$I4$	-0.26
$I5$	$8.2 \cdot 10^{-3}$
$\langle\beta_x\rangle$	8.7
$\langle\beta_y\rangle$	9.0

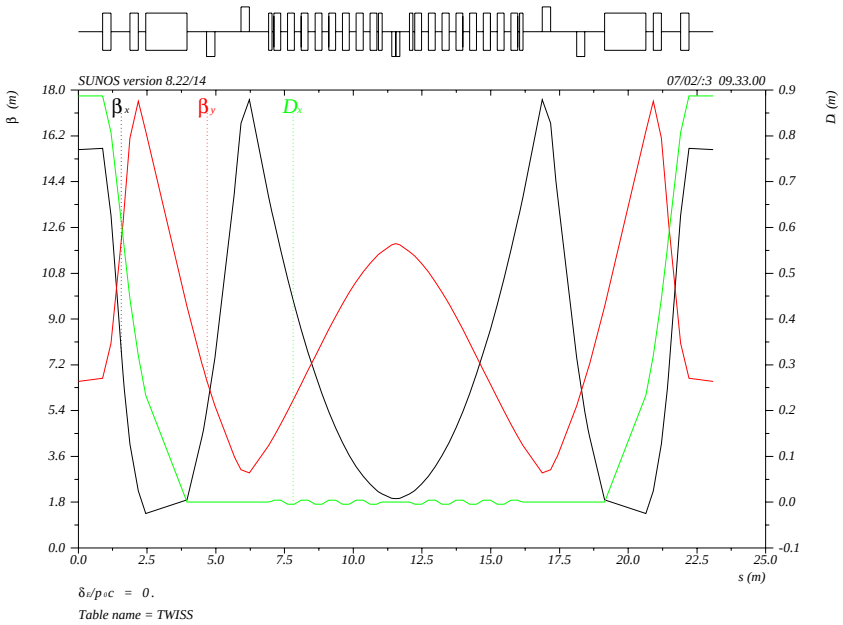

Figure 1: Lattice functions in one wiggler cell.

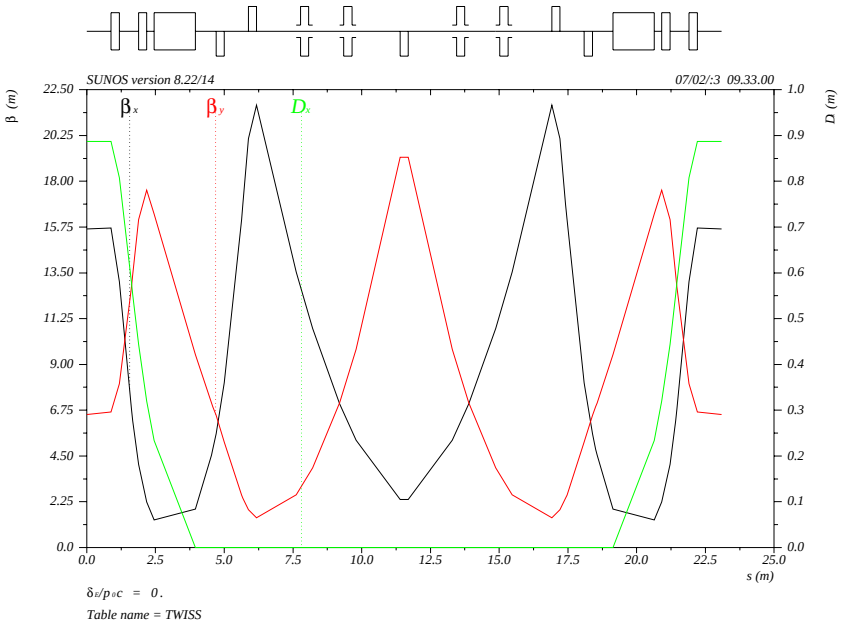

Figure 2: Lattice functions in the RF cell.

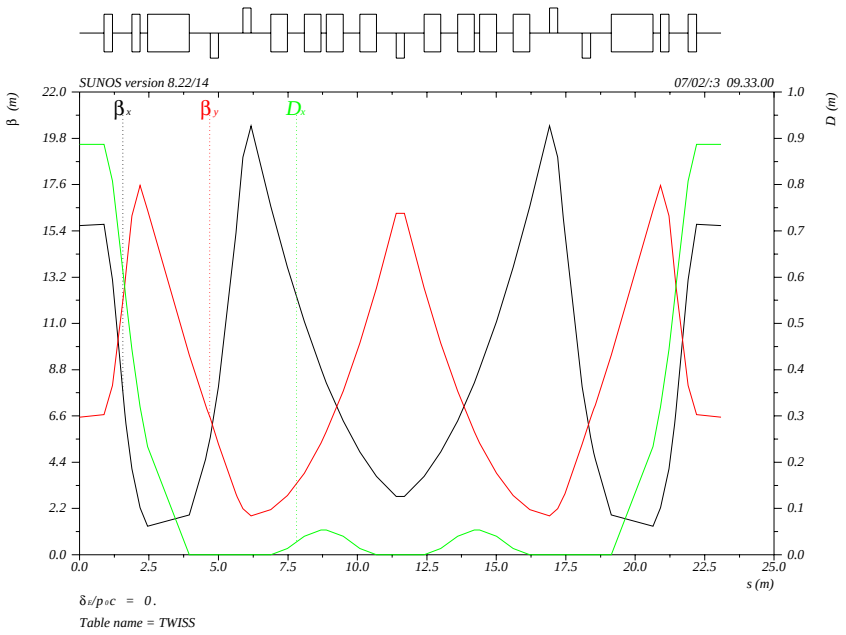

Figure 3: Lattice functions in the chicane cell.

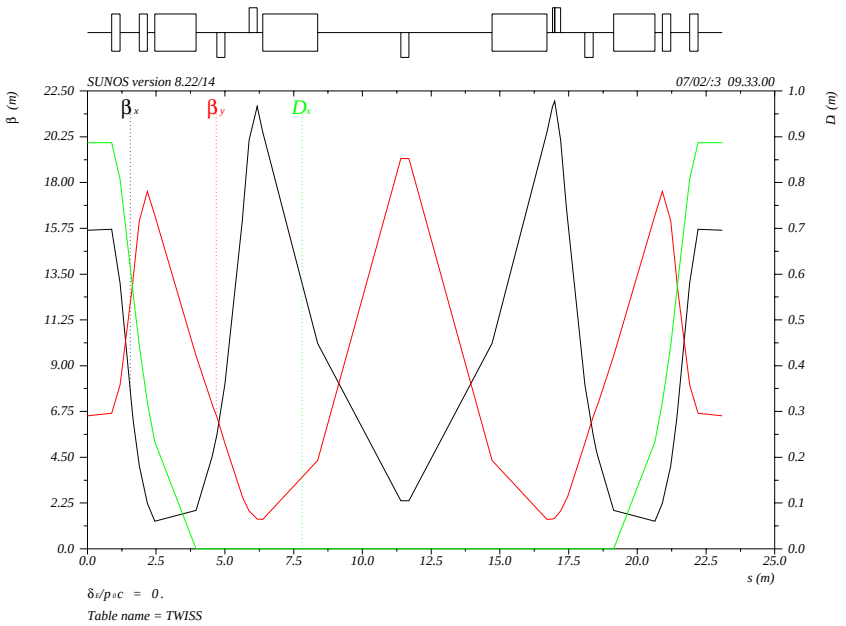

Figure 4: Lattice functions in the injection cell.

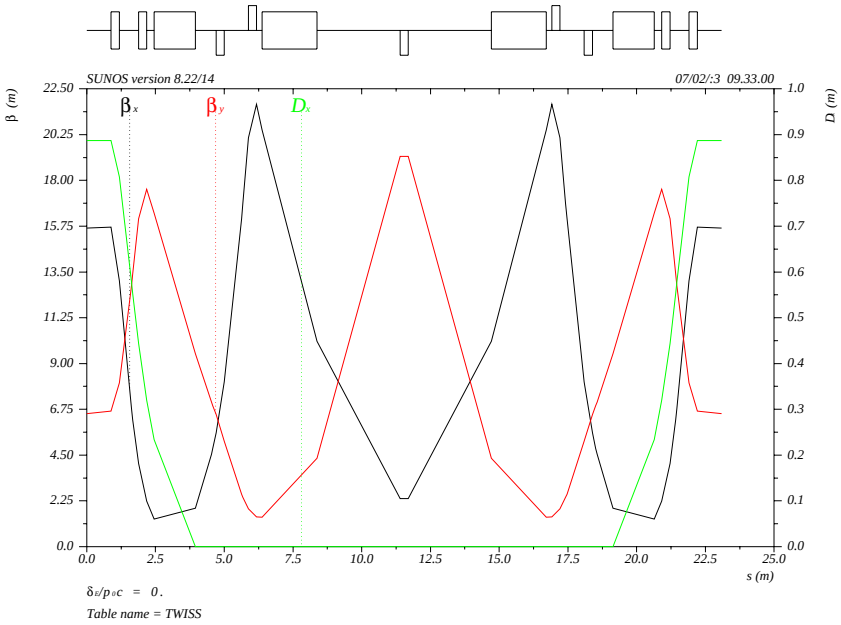

Figure 5: Lattice functions the extraction cell.

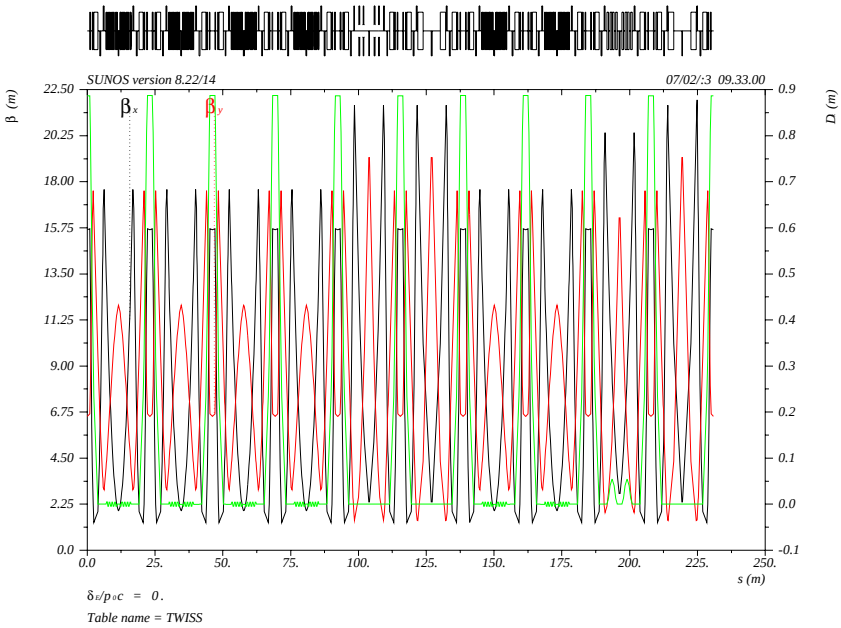

Figure 6: Lattice functions around the whole ring.

ties driven by modes in the cavities have yet to be carried out for the pre-damping ring, though we note that in the case of the main damping rings, only a few modes transverse and longitudinally are above the damping threshold [5], and growth rates for these modes can readily be dealt with by feedback systems.

2.2 Chicanes

The present design uses two separate chicanes, each being identical in design to that used in the main damping ring, and allowing adjustment of the circumference of ± 2 mm each. Thus, the total circumference adjustment range is ± 4 mm. The use of the same system in the pre-damping ring as in the main damping ring in itself brings some benefits. Using two chicanes rather than one eases the technical requirements and minimizes the retuning required in the circumference adjustment; it also allows the symmetry of the cell to be maintained.

2.3 Injection/Extraction Systems

We have assumed the same design for the injection / extraction kickers and septa as given in the NLC ZDR [6]; the kickers and septa are each 2 m long, the kickers providing a deflection of 8 mrad (injection) and 6.6 mrad (extraction), and the septa a deflection of 150 mrad. The central defocusing quadrupole provides additional bending for the injected / extracted beam. The circumference of the lattice allows for a kicker rise / fall time of 119 ns. With the present design, the kicked beam is 81 mm off-axis relative to the stored beam at the entrance to the septum (see Fig. 7). At the location of the next quadrupole following the last septum in the direction of the extracted beam, the kicked beam is 298 mm off-axis, with respect to the stored beam. The technical constraints so far look reasonable.

2.4 Overall Structure

The overall structure of the pre-damping ring lattice is shown in Figure 6. The sequence of cells can be chosen for practical convenience: there are no fundamental lattice issues. The only constraint is that the RF cell has to be located anywhere from the injection to the extraction straight (following the direction of the beam), where the cavities will not be subject to any transient beam loading resulting from in injection / extraction cycle. Otherwise the order of the cells can be chosen depending on convenience for engineering

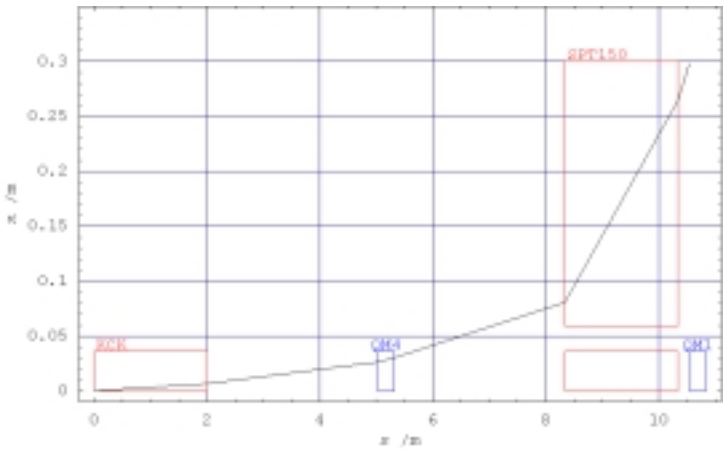

Figure 7: Extraction

purposes (there might be additional constraints where to put injection and extraction with respect to each other depending on the layout of the whole injector complex).

3 Dynamics and Acceptance

3.1 Chromatic Properties

The achromat is designed to provide large horizontal dispersion and good separation of the horizontal and vertical beta functions between the dipoles, to allow correction of the chromaticity with moderate sextupole strengths. Constraining the beta functions to low values throughout the lattice helps keep the natural chromaticity of the lattice low. Harmonic sextupole magnets, placed in regions of zero dispersion, can be used to correct nonlinear betatron parameters.

Figure 8 shows the variation in tune with momentum up to $\pm 2\,\%$ momentum deviation. The tune variation looks sufficiently small to allow reasonable dynamic momentum acceptance. We have not yet carried out a completely rigorous analysis of the harmonic sextupole tuning, and further optimization may be possible.

While producing Fig. 8 a bug was found in MAD. The chromaticities calculated by MAD (using the `TWISS` command) actually did not correspond to the slope at $\frac{\Delta p}{p} = 0$. For the sextupole strengths used to produce the graph MAD calculates chromaticities of $\xi_x = 1.9$ and $\xi_y = -2.7$. The strength

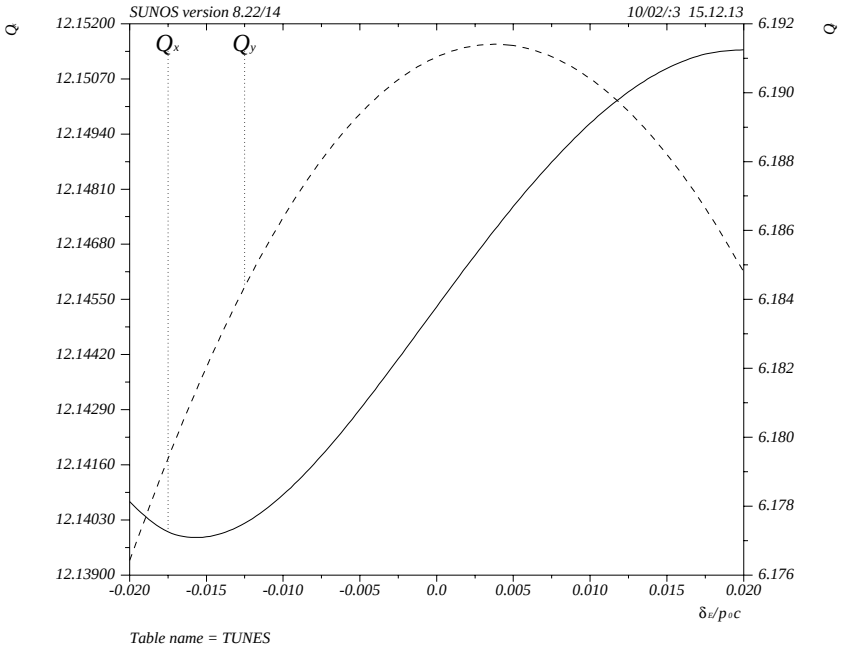

Figure 8: Tune shift with momentum up to $\pm 2\,\%$ momentum deviation.

of the sextupoles has been optimized to achieve a fairly small change in tune over a range of $\pm 2\,\%$ momentum deviation instead of having zero chromaticity according to `TWISS`.

The working point in tune space is shown in Fig. 9. We are not overly concerned about the proximity to coupling resonances: low betatron coupling is not a performance requirement for the pre-damping ring, since the specification on extracted emittances places equal upper limits in the two transverse planes.

3.2 Acceptance

As we have already mentioned, the specified acceptance of the ring is for an edge emittance of 45,000 mm mrad and half-width energy spread of 1.5 %. Figure 10 shows the required acceptance for the wiggler and RF cell. In the horizontal plane the aperture is slightly too small in the arcs. As this is at a place with high dispersion only particles at large amplitude and large energy offset would get scraped. Nevertheless we are thinking about increasing the aperture there by a couple of mm. In the vertical plane the aperture is very tight between the wiggler and the adjacent quadrupole. To

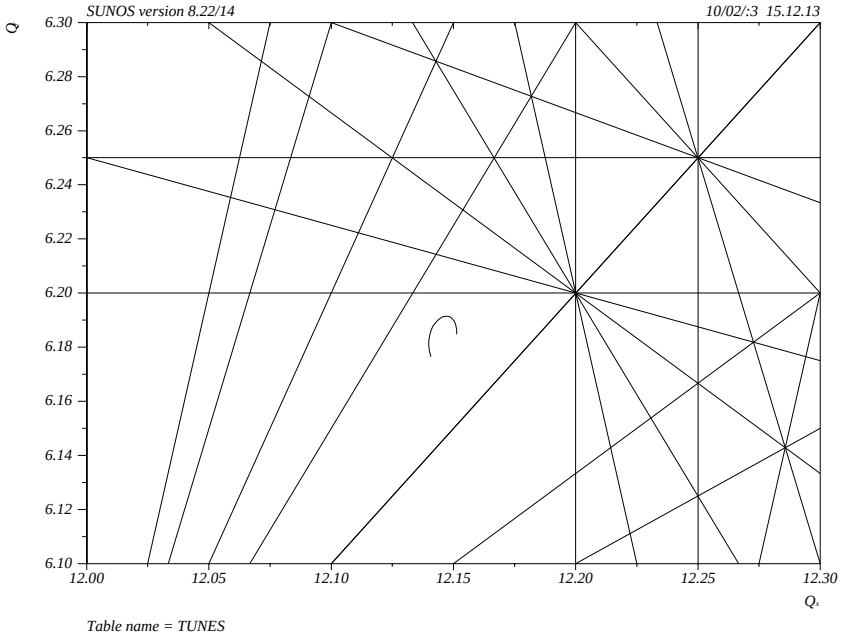

Figure 9: Working point in tune space. The nominal working point is (12.145, 6.191): the curved line shows variation in tunes up to $\pm 2\,\%$ momentum deviation. Resonance lines up to fifth order are shown.

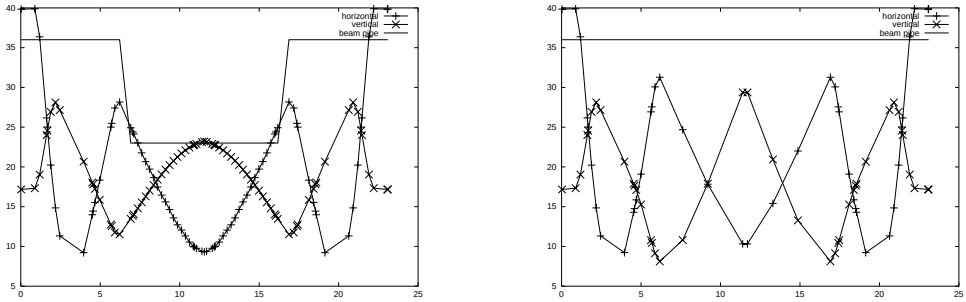

Figure 10: Required acceptance in the wiggler (left) and the RF (right) cells.

avoid any problems the aperture will need to be opened up immediately following the wiggler and not closer to the quadrupole as depicted here.

The present specification of the lattice is for a transverse acceptance corresponding to an edge emittance of 45,000 mm mrad; this is derived from the nominal injected beam edge emittance of 30,000 mm mrad, plus 50 % to allow for mismatches and jitter. We note that a particle at the dynamic acceptance limit has a maximum offset from the design orbit given by:

$$\hat{x} = \sqrt{2\beta\varepsilon_{edge}} + \eta\delta \tag{1}$$

where η is the dispersion, and δ is the momentum deviation.

The specified energy acceptance is ± 1.5 %. This again includes a margin of 50 % over the nominal beam properties (1 % half-width energy spread) to allow for jitter. The equilibrium bunch length is 5.2 mm with an energy spread of 0.089 % (see Tab. 2): thus, we expect that soon after injection, the bunch length is likely to filament to around 87 mm. With an RF wavelength of 420 mm, and rapid longitudinal damping, this is not anticipated to be a problem.

3.3 Dynamic Aperture

To assist with injection efficiency, the dynamic aperture of the lattice is improved through the use of harmonic sextupoles.

Horizontal and vertical phase space portraits for on-momentum particles are shown in Fig. 11.

The dynamic apertures, for particles with zero and ± 1.5 % momentum deviation, are shown in Fig. 12. The dynamic aperture is calculated by tracking 200 turns, with the observation point in the quadrupole magnet next to the septum in the injection straight. The tracking is done with

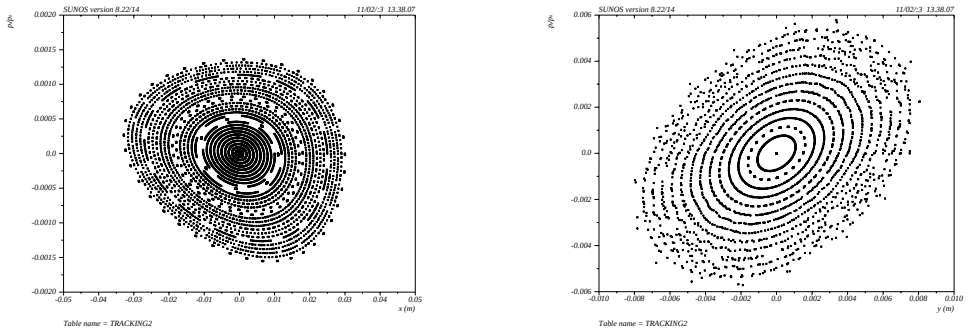

Figure 11: Horizontal (left) and vertical (right) phase space portraits for on-momentum particles with apertures.

physical apertures to model the size of the beam pipe. Without the physical apertures the dynamic aperture is much larger (see Fig. 13). At this location, the horizontal beta function has a value of 2 m, the vertical beta function is 1.5 m, and the horizontal dispersion is zero. The required acceptance also shown in Fig. 12 is calculated using these values in Eq. 1, with an edge acceptance of 45,000 mm mrad. The dynamic aperture appears to be beyond the required limit. We have not so far included multipole field errors in the magnets, although we do not expect this to affect the dynamic aperture to such an extent that the specified acceptance cannot be achieved, especially as the acceptance is mainly limited by the physical aperture and not by dynamics. We have so far carried out only a preliminary optimization of the dynamic aperture. It is to be expected that with more work, optimizing the the locations and strengths of the harmonic sextupoles, the dynamic aperture may be improved.

We also had a short look at the frequency map. They are calculated assuming reasonable errors (the same as for the ALS are used) as frequency maps without any machine errors are not very meaningful. The frequency map was calculated without any corrections and with the tunes being corrected back to the nominal values The results are shown in Fig. 14 in tune space and in Fig. 15 in transverse phase space. The one with the uncorrected tune shows no strong resonances within the required aperture. The one with the corrected tune looks slightly worse but so far no effort has been made to optimize the tunes beyond not having them on resonances of order three or less. Both figures were provided by Christoph Steier.

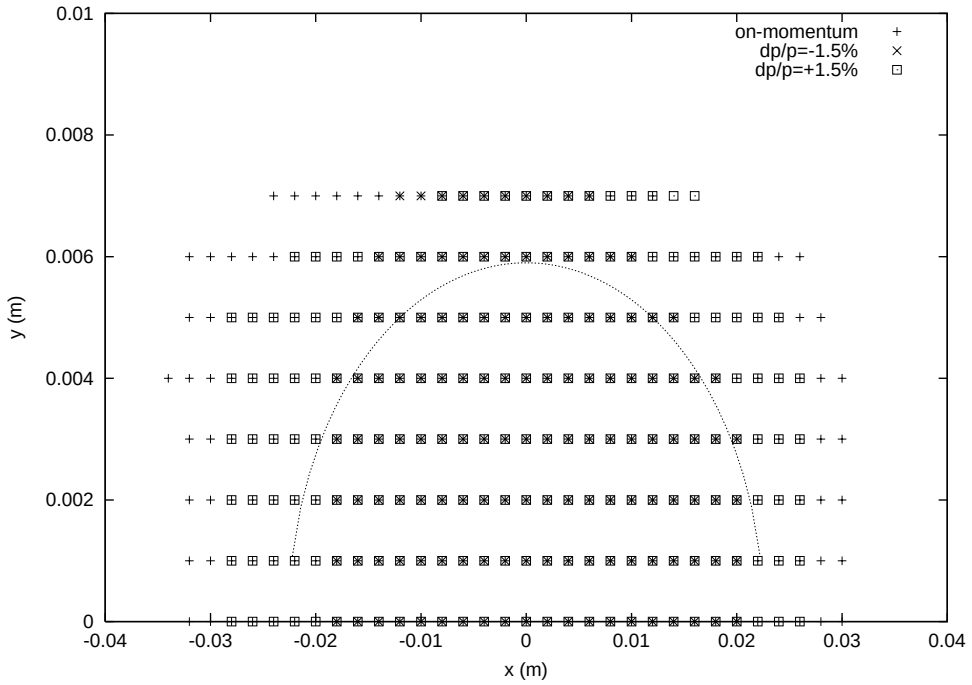

Figure 12: Dynamic apertures for particles with zero and $\pm 1.5\%$ momentum deviation with apertures.

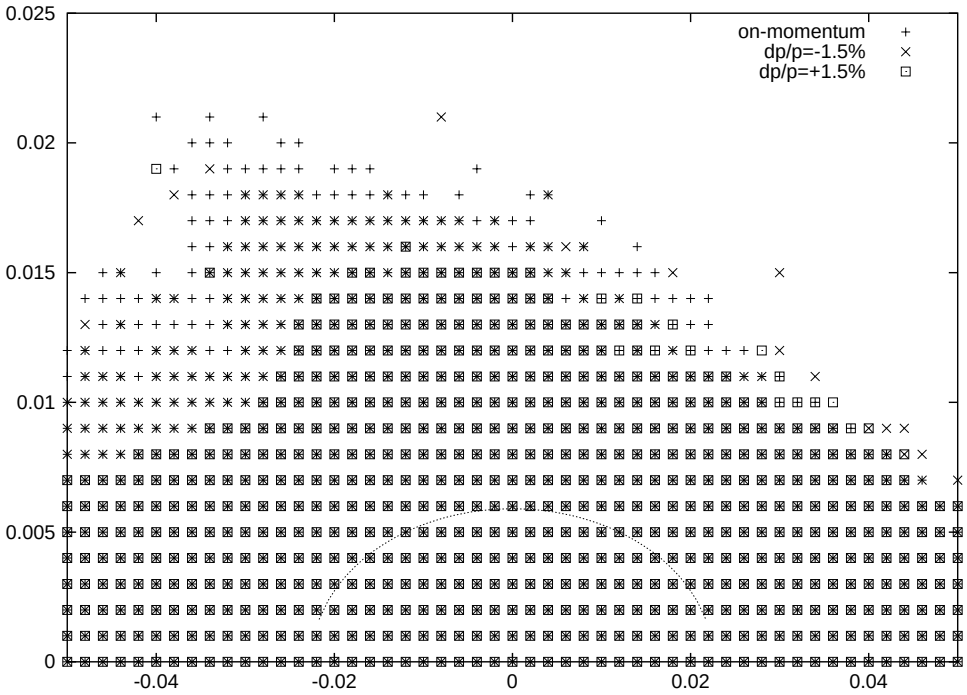

Figure 13: Dynamic apertures for particles with zero and $\pm 1.5\,\%$ momentum deviation without apertures.

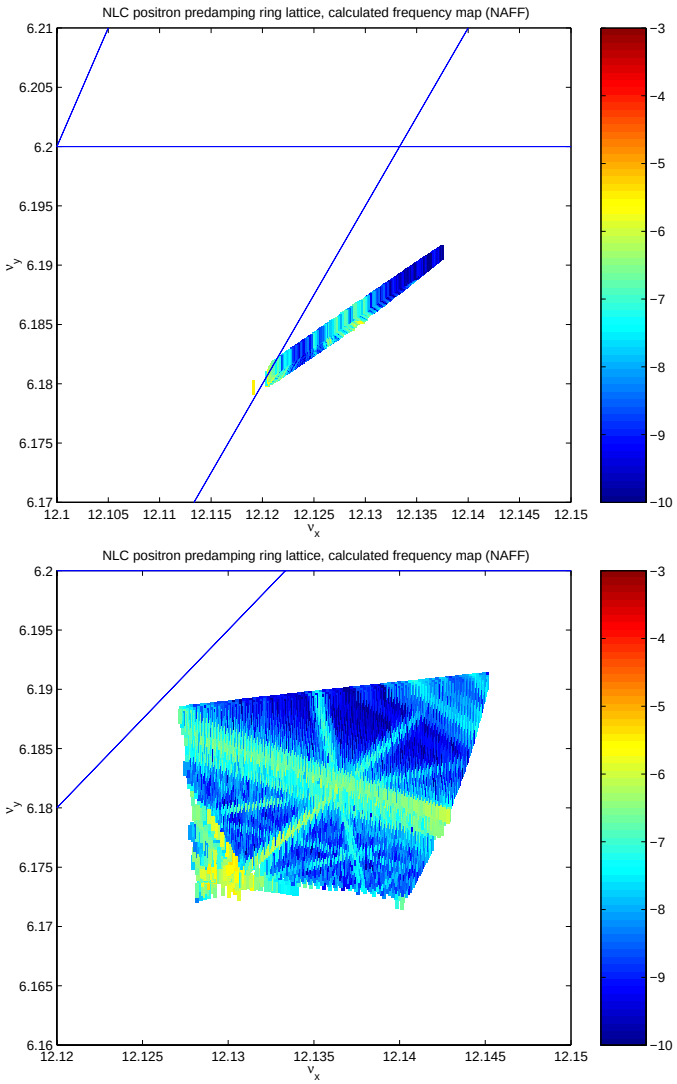

Figure 14: Frequency map in tune space without (top) and with (bottom) tune correction. Resonances lines up to third order are shown.

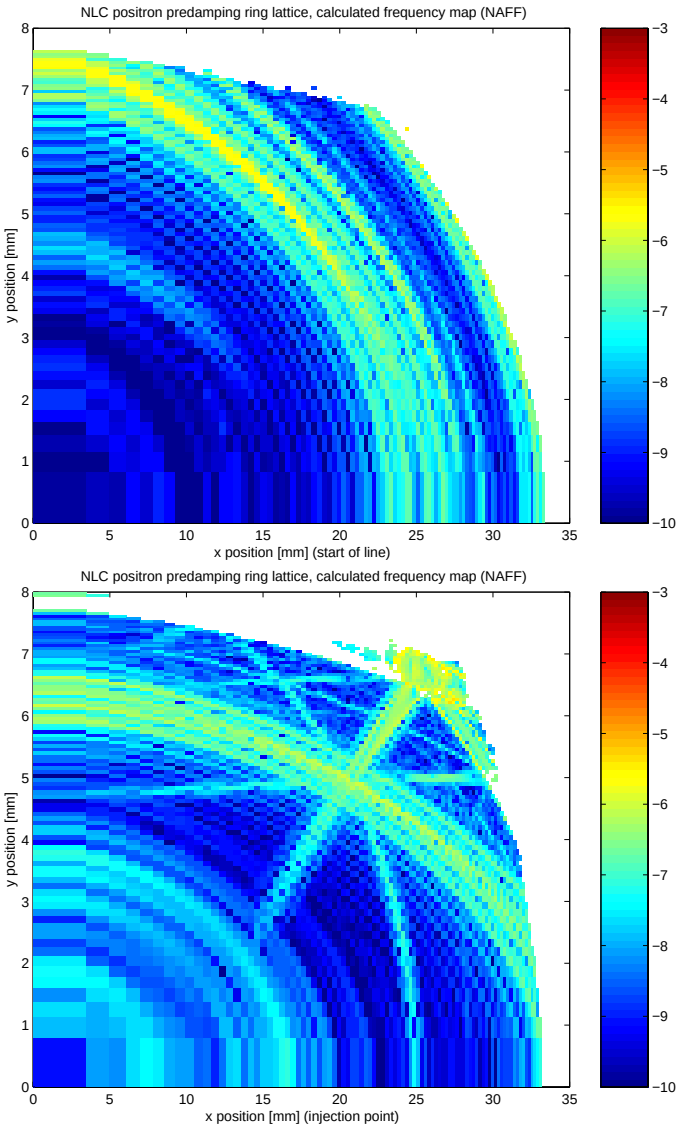

Figure 15: Frequency map in transverse phase space without (top) and with (bottom) tune correction.

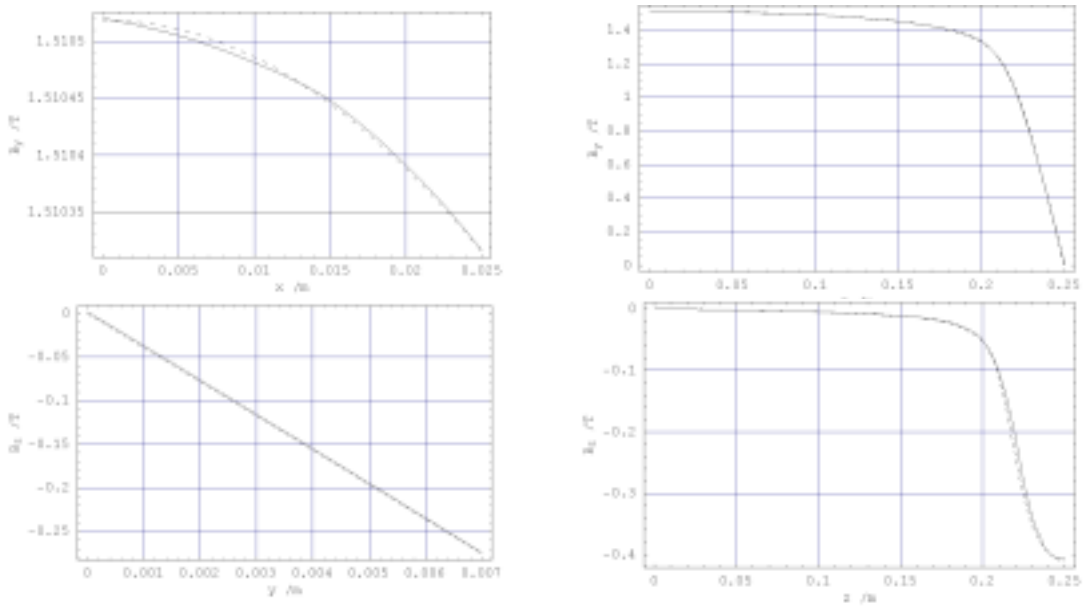

Figure 16: Sample field fits.

4 Wiggler

A magnetic design and field map for the hybrid technology damping wiggler has been produced [7]. For analysis of the dynamics, we have followed the same approach as in [2], where more details of the technique are given. Briefly, this involves fitting a set of cylindrical modes to the field map, and then using the mode coefficients in a symplectic integrator. Sample field fits are shown in Fig. 16. The results of symplectic tracking through a single period of the wiggler are shown in Fig. 17. Because of the detailed nature of the field fit, the tracking is too slow to be practical for dynamic aperture calculations, and we have therefore approximated the dynamics using thin octupole and dodecapole components in the wiggler: the dynamics of this model are the lines shown in Fig. 17, which match very closely the points obtained by tracking. The integrated octupole strength per wiggler period is small ($k_3 l = -5.2\,\mathrm{m}^{-3}$), and the dodecapole somewhat larger ($k_5 l = 72600\,\mathrm{m}^{-5}$). We note that this is not a completely rigorous model of the wiggler dynamics, since the nonlinear effects of the wiggler field cannot in general be reproduced using thin multipoles. A more careful analysis is planned, but for the present purposes the multipole model appears to work well enough to give the dynamic aperture calculations some credibility.

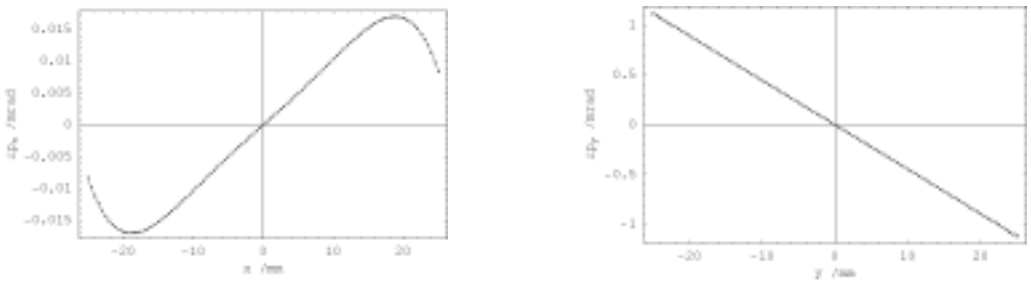

Figure 17: Results of symplectic tracking through a single wiggler period.

It is important to observe that the horizontal and vertical focusing from the wiggler differs from that expected from a hard-edged dipole model of the wiggler. The small amount of horizontal focusing comes from a feed-down of the local sextupole component in the wiggler. The vertical focusing is significantly different from that expected given the peak field and period, and is related to the integrated square of the vertical field component. From Fig. 16, it is clear that the integrated field from the field map ($1.907\,\mathrm{T}^2\mathrm{m}$) is much larger than that found using the usual lattice model with pole lengths that are a quarter of the wiggler period ($0.98\,\mathrm{T}^2\mathrm{m}$). We find that by raising the peak field in the lattice model from 1.4 T to 1.956 T, and including a small focusing ($k_1 l = -0.008\,\mathrm{m}^{-1}$ per period), we produce the horizontal and vertical focusing and the integrated field found from the field map. Using the correct integrated field is also important for finding the correct energy loss per turn of particles in the ring, and this in turn has an important impact on the damping times and the natural emittance.

Name	Type	Location	Length	Pole-tip radius	Pole-tip field	Quadrupole gradient[a]	Sextupole gradient[b]	Count
BB	Dipole		1.5	0.04	1.38			20
BBCHP	Dipole	Chicane	0.6	0.04	0.98			4
BBCHM	Dipole	Chicane	0.6	0.04	−0.98			4
QAF	Quadrupole	Achromat[c]	0.3	0.04	0.531	2.01		20
QAD	Quadrupole	Achromat[c]	0.3	0.04	−0.472	−1.79		20
QM0W	Quadrupole	Wiggler cell straight	0.3	0.04	−0.006	−0.02		12
QM1W	Quadrupole	Wiggler cell straight	0.3	0.04	0.447	1.69		12
QM4W	Quadrupole	Wiggler cell straight	0.3	0.04	−0.060	−0.23		6
QM0CH	Quadrupole	Chicane cell straight	0.3	0.04	−0.113	−0.43		2
QM1CH	Quadrupole	Chicane cell straight	0.3	0.04	0.467	1.77		2
QM4CH	Quadrupole	Chicane cell straight	0.3	0.04	−0.289	−1.10		1
QM0	Quadrupole	Straight	0.3	0.04	−0.158	−0.60		6
QM1	Quadrupole	Straight	0.3	0.04	0.488	1.84		6
QM4	Quadrupole	Straight	0.3	0.05	−0.399	−1.21		3
SX	Sextupole	Achromat	0.05	0.04	0.417		78.9	10
SY	Sextupole	Achromat	0.05	0.04	−0.278		−52.7	20
S1W	Sextupole	Wiggler cell straight	0.05	0.04	−0.528		−100.0	12
S2W	Sextupole	Wiggler cell straight	0.05	0.04	0.228		43.1	12
S1	Sextupole	Straight	0.05	0.04	−0.449		−84.8	8
S2	Sextupole	Straight	0.05	0.04	0.192		36.4	8

[a] Normalized: $(\partial B_y/\partial x)/B\rho$
[b] Normalized: $(\partial^2 B_y/\partial^2 x)/B\rho$
[c] horizontally offset by 1.5 mm

Acknowledgments

We would like to thank Christoph Steier for calculating the frequency map for us.

References

[1] Andrzej Wolski. A new structure for the NLC positron pre-damping ring lattice. CBP Tech Note 47, LCC-0066, Lawrence Berkeley National Laboratory, June 2001.

[2] M.D. Woodley and A. Wolski. The NLC Main Damping Ring lattice, February 2003. LCC 0113, February 2003.

[3] R.A. Rimmer et al. An RF cavity for the NLC damping rings. In *Proceedings of the 19th Particle Accelerator Conference*, Chicago, USA, May 2001.

[4] Robert A. Rimmer. RF cavity R&D at LBNL for the NLC Damping Rings, FY2000/2001. LCC 0072, Lawrence Berkeley National Laboratory, October 2001.

[5] Stefano de Santis. Coupled bunch instabilities in the NLC damping rings. LCC 0069, Lawrence Berkeley National Laboratory, April 2001.

[6] NLC Design Group. Zeroth-order design report for the Next Linear Collider. SLAC Report 474, SLAC, May 1996. LBNL-PUB-5424.

[7] S. Marks, private communication.